Ion heat and toroidal momentum transport studies in the H-mode transport barrier of ASDEX Upgrade

E. Viezzer[1,2], M. Cavedon[1,3], E. Fable[1], A. Snicker[1], C. Angioni[1], R. Dux[1], S. Fietz[1], F. M. Laggner[4], R. M. McDermott[1], T. Pütterich[1], T. Odstrčil[1,3], F. Ryter[1], E. Wolfrum[1], the ASDEX Upgrade Team[1] and the EUROfusion MST1 Team[5]

[1]Max-Planck-Institut für Plasmaphysik, Boltzmannstr. 2, 85748 Garching, Germany
[2]Dept. of Atomic, Molecular and Nuclear Physics, University of Seville, Spain
[3]Physik-Department E28, Technische Universität München, Garching, Germany
[4]Institute of Applied Physics, TU Wien, Fusion@ÖAW, Vienna, Austria
[5]See appendix of H. Meyer et al. (OV/P-12) Proc. 26th IAEA FEC 2016, Kyoto, Japan

Corresponding Author: Eleonora.Viezzer@ipp.mpg.de

Abstract:
The ion heat and toroidal momentum transport at the plasma edge of ASDEX Upgrade (AUG) H-mode plasmas are investigated by combining measurements with interpretive and predictive modelling. The experimentally determined ion heat diffusivities, χ_i, are compared to neoclassical theory and the impact of edge localized modes (ELMs) on the edge ion heat transport level is studied in detail. In all analyzed cases the pre-ELM χ_i in the pedestal is close to the neoclassical prediction within the experimental uncertainties. During the ELM crash, the ion heat transport is increased by an order of magnitude due to the outward heat pulse propagation caused by the ELM. The perturbed heat flux is first increased at the separatrix and is then observed to penetrate inwards, i.e. first the separatrix ion temperature increases at the ELM onset, leading to a flatter ion temperature gradient, followed by a decrease of the whole edge profile up to the pedestal top. The ion heat transport is restored to its pre-ELM neoclassical level 3–4 ms after the ELM crash.
The edge impurity toroidal rotation shows a dependence on collisionality, with negative (counter-current) values at low collisionality, and positive (co-current) values at high collisionality. Modelling of the edge toroidal rotation based on the toroidal torque balance equation including diffusion, pinch and external momentum sources indicates that diffusion and the external sources are the dominant players at both low and high collisionality. The sign change of the impurity toroidal rotation observed at low collisionality can be explained by a negative edge torque combined with a large differential toroidal rotation, while the main ion toroidal rotation is almost unaffected.

1 Introduction

Plasma turbulence is driven by spatial inhomogeneities in the plasma temperature and density and leads to electron and ion heat diffusivities that exceed the neoclassical level,

which is typically observed in tokamak plasmas. At the onset of the high confinement mode (H-mode), the edge turbulence level is strongly reduced and a steep edge pressure gradient is build up. The H-mode is accompanied by the occurrence of edge localized modes (ELMs), which are magnetohydronamic instabilities that expel particles and energy from the pedestal region, leading to a transient degradation of the H-mode transport barrier. Understanding the transport processes in the pedestal is essential for a reliable scaling to next step fusion devices.

Extensive studies of the heat transport in the plasma core have been carried out in the past [1–3]. The pedestal, with its small spatial width (typically 1.5–2 cm at ASDEX Upgrade, AUG) and its fast temporal changes due to the ELMs, is a more challenging region to analyze. Thus, little focus has so far been directed to this region due to lack of high-resolution diagnostics. Extensive effort has been made in the past years to upgrade the diagnostics at the plasma edge to meet the needs required for resolving the fast dynamics and the steep gradients of the pedestal. The unique edge diagnostic suite available at AUG allows us to measure the edge plasma profiles on a sub-ms to ms time scale with a spatial resolution of less than 5 mm [4]. The comprehensive set of diagnostics makes it ideal to study the recovery of the profiles after an ELM crash.

This contribution analyses the ion heat and momentum transport at the plasma edge. During the inter-ELM phase the ion heat transport is close to the neoclassical level, while during the ELM crash an increased level is observed due to the outward propagation of the heat pulse caused by each ELM. Modelling of the toroidal rotation suggests that diffusion and external sources are important and that the neoclassical toroidal viscous torque and residual stress driven by turbulence play a minor role in the discharges analyzed here.

2 Edge ion heat transport: comparison of experiment and modelling

The evaluation of the heat transport coefficients requires a good separation between electron and ion heat fluxes. Low collisionality plasmas facilitate this kind of analysis as the electron-ion energy exchange term in the power balance becomes small. Dedicated discharges at low collisionality were carried out at AUG to study the ion heat transport at the plasma edge [6]. The experiments are type-I ELMy H-mode plasmas with a toroidal magnetic field on-axis of -2.5 T, a plasma current of 1 MA, a core line-averaged density varying from 6.6.–7.7$\times 10^{19}$ m^{-3} and a total heating power of 8.7 MW, distributed between neutral beam injection (7.1 MW) and electron cyclotron resonance heating (1.6 MW). The collisionality in the pedestal region (at $\rho_{pol} = 0.97$) varied from 0.2–0.5 from shot to shot. Figure 1 shows the pre-ELM profiles of the electron temperature (T_e), density (n_e), ion temperature (T_i) and toroidal impurity rotation (v_{tor}, in this case measured on B^{5+}) for a low and high collisionality case.

The ion heat diffusivity profiles are determined via power balance analysis using the 1.5D transport code ASTRA [5], which solves the time dependent, flux surface averaged heat transport equation. The ion and electron energy sources and the heat exchange term

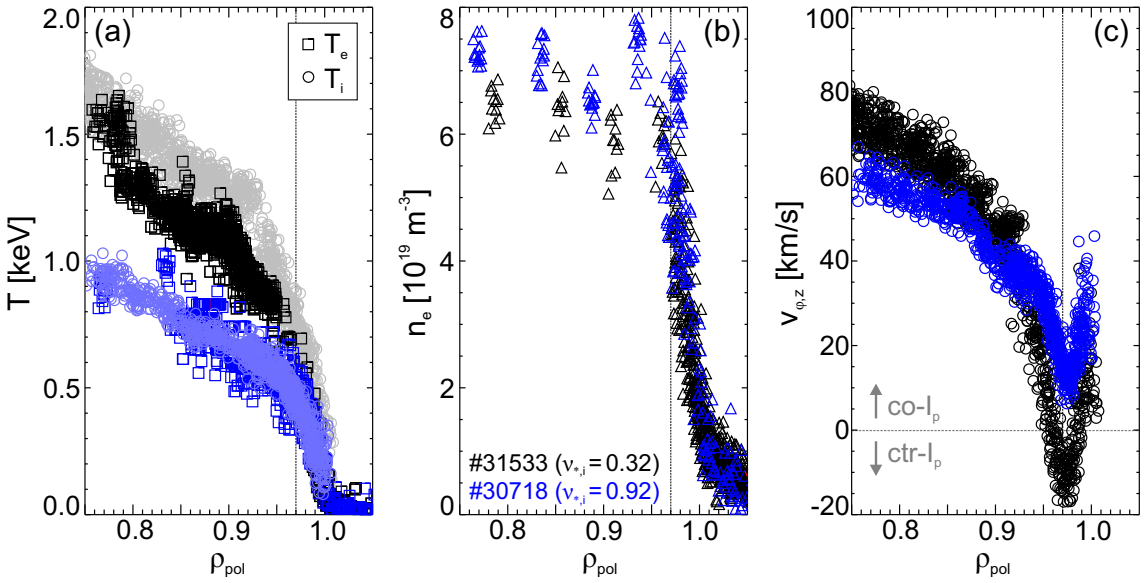

FIG. 1: Pre-ELM profiles of (a) T_e and T_i, (b) n_e, (c) v_{tor} of B^{5+}.

between ions and electrons determine the ion and electron heat fluxes. The electron heating power includes the ohmic heating power, the collisional heat exchange between ions and electrons, the radiated power, power losses due to atomic processes and the auxiliary power to the electron channel. Similarly, the ion energy source depends on the electron-ion exchange rate, losses due to atomic processes and auxiliary ion heating. The heat flux is related to the temperature gradient via the heat conductivity and is determined by the energy sources; $Q = -n\chi(\rho)\partial T/\partial\rho$. In steady state the heat flux corresponds to the integral of the sources. Interpretive modelling with ASTRA enables the determination of the ion heat conductivity using power balance analysis.

Figure 2 shows the ion heat conductivity at the plasma edge. The neoclassical prediction simulated with NEOART is shown in blue, while in red and green the NEO and NCLASS calculations are shown. The power balance analysis yields an edge ion heat conductivity on the order of ∼0.6–0.7 m^2/s. The temporal evolution of T_i within the analyzed time window is taken into account for the evaluation of the heat flux and χ_i plotted in figure 2 represents the temporal average.

The transport analysis was extended to plasmas with varying collisionality. Note, however, that at higher collisionality the determination of the ion heat flux and thus, χ_i has a significantly larger error bar as the coupling between ions and electrons is larger and therefore, the electron ion heat exchange term is not negligibly small. All analyzed discharges feature a low ELM frequency (<100 Hz) to allow for an inter-ELM evaluation of the ion heat transport. In figure 2(b), the χ_i profile for a high collisionality case is shown. Similarly, χ_i in the core exceeds the neoclassical predictions while in the pedestal the ion heat transport approaches the neoclassical level.

Figure 3(a) shows the pedestal ion heat conductivity as a function of the main ion collisionality. Both values are taken at the radial position ρ_{pol}=0.97. The experimentally determined values of χ_i^{exp} are shown in black, while the neoclassical predictions calcu-

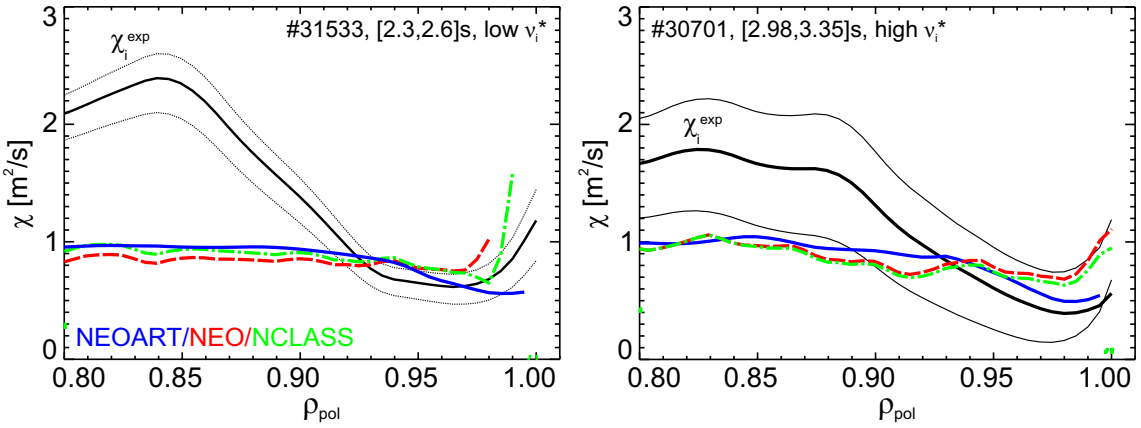

FIG. 2: Experimentally determined ion heat diffusivity using power balance analysis (χ_i^{exp}) in black, neoclassical predictions calculated with NEOART (blue), NEO (red, dashed line) and NCLASS (green, dashed-dotted line).

lated with NEOART are shown in blue. For the two cases discussed above, the NEO and NCLASS values are shown in red and green, respectively.
For a comparison, figure 3(b) shows the electron heat transport coefficients as determined via power balance analysis (black stars). Note that for χ_e the evaluation depends on the radiated power, which has large uncertainties. The neoclassical values of χ_e are marked as blue circles. While at the plasma edge the ion heat transport is close to the neoclassical level, the electron heat transport exceeds the neoclassical predictions by one to two orders of magnitude.

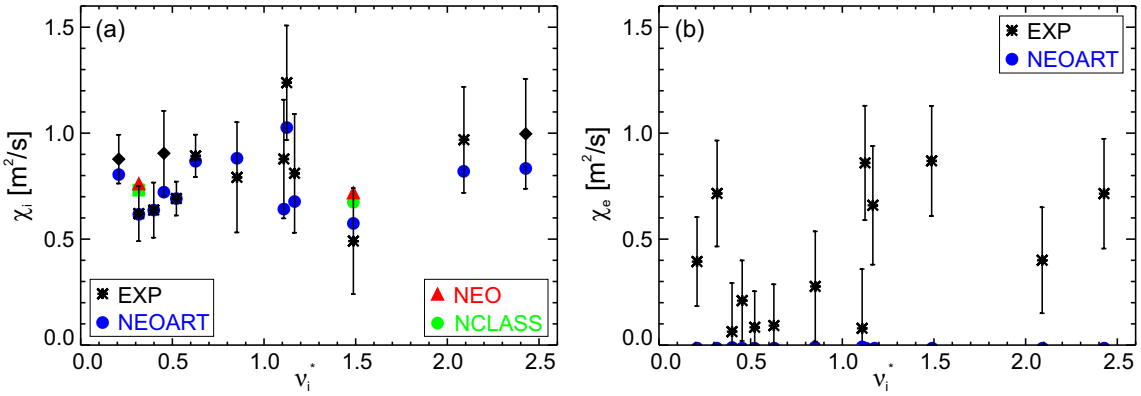

FIG. 3: Heat diffusivities as a function of the main ion collisionality (at $\rho_{pol} = 0.97$): (a) ions, (b) electrons.

2.1 Evolution during the ELM cycle

The recent upgrade of the edge CXRS diagnostics [7] allows us to measure the dynamics of the ion temperature at AUG with unprecendented time resolution down to 70 μs. In

order to improve the signal-to-noise ratio, helium seeding is required and therefore, it is not a standard diagnostic. A dedicated type-I ELMy H-mode discharge was carried out to measure the evolution of the ion temperature, impurity density and flows, and the edge radial electric field [8]. Here, the plasma current was I_p = 0.8 MA, the toroidal magnetic field on-axis B_t = -2.5 T, the core line-averaged density 6.9×10^{19} m^{-3} and the total input power was 5.8 MW (4.8 MW NBI, 1 MW ECRH). The ELM frequency was constant at around 85 Hz. The measured data taken during the time window [3.5, 5.5] s was synchronized with respect to the onset of the ELMs.

The ion heat transport modelling using the ASTRA code has been applied to the entire ELM cycle. As the whole profile is needed for the simulations, the measurements of the fast edge CXRS system (in this case rebinned to 100 μs to match the time basis of the n_e measurements) have been combined with the slower standard edge CXRS diagnostics (temporal resolution 2.3 ms) and the core CXRS system (set to 5 ms in this discharge). To this end, the measurements of the slower systems have been fitted for various time windows during the ELM cycle and mapped onto the time basis of the fast system. Care has been taken to exclude the impact of the ELMs on the pre- and post-ELM profiles. Note that for the core system the ELM averaged profile is used due to the limited time resolution.

Figure 4 shows (a) the ion temperature profiles, (b) the ion heat diffusivities and (c) the surface-integrated ion heat flux Q_i for four time points during the ELM cycle. The area highlighted in gray is the region where the measurements of the fast edge system overlap with those of the slower ones. As the profiles are interpolated in order to have a combined core and edge profile, the gradients in this region are unphysical. Note that the χ_i and Q_i profile highlighted in red are measured during the ELM crash and have been divided by a factor of 10. In figure 4(b) the neoclassical χ_i profile is marked by a dashed line. For clarity, only the profile of the first time point is shown.

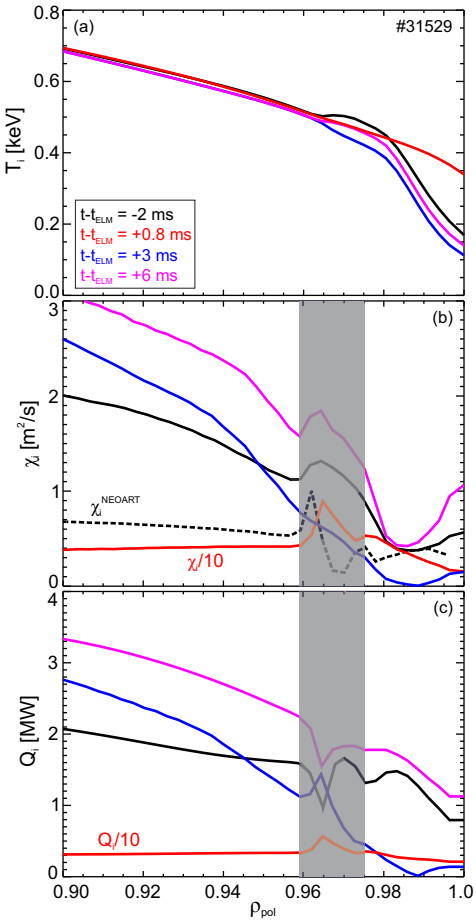

FIG. 4: Profiles for four time points during the ELM cycle: (a) T_i, (b) χ_i determined via power balance and χ_i^{NEOART} calculated from neoclassical theory, (c) heat flux Q_i.

In the core, turbulent transport dominates and leads to a strong deviation of χ_i from neoclassical theory while in the edge transport barrier χ_i approaches the neoclassical level (except for the time points during the ELM). Note that very close to the separatrix, the ordering of neoclassical theory breaks down and does not describe the increase of χ_i for ρ_{pol}>0.997.

Figure 5 shows the evolution of (a) T_i and (b) the ratio between the experimentally

determined χ_i^{PB} and the neoclassical χ_i^{neo} during the ELM cycle, (c) the thermo-currents in the inner divertor used as an ELM monitoring signal. At the ELM onset, the separatrix T_i increases, leading to a reduced gradient in the pedestal [8], similar to observations at DIII-D [9]. Shortly after the initial separatrix increase, the whole profile drops and then the T_i pedestal starts to build up again. The pre-ELM profile is restored 3–4 ms after the ELM crash.

As shown before, the pre-ELM values of χ_i at the plasma edge are in agreement with the neoclassical values, while during the crash χ_i is increased due to anomalous transport caused by the ELM. The perturbed heat flux is first increased at the very edge of the plasma and then penetrates inwards. Note that later in the ELM cycle (t-t$_{ELM}$>6 ms), χ_i at the very edge of the plasma is increased compared to the neoclassical calculation (see figure 5(b)), indicating that close to the separatrix anomalous transport may become important. It should also be noted that during the inter-ELM phase the uncertainties of the separatrix T_i are large due to uncertainties in the equilibrium mapping and in the alignment and due to a low signal-to-noise ratio. Extending the CXRS measurements to the SOL and combining them with other SOL diagnostics capable of measuring T_i would help in quantifying χ_i at the separatrix and beyond.

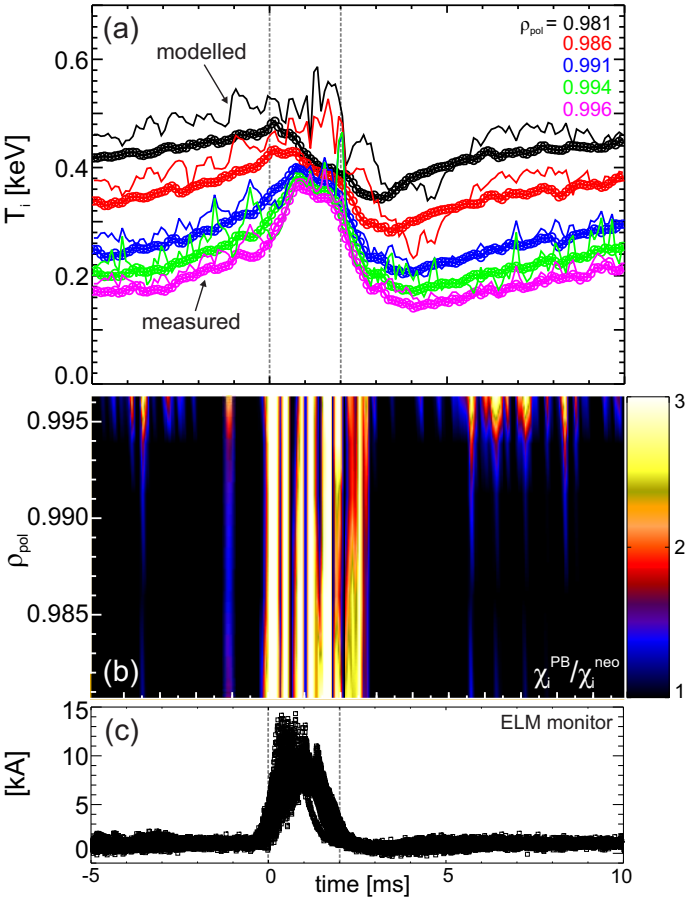

FIG. 5: Temporal evolution of (a) T_i and (b) χ_i/χ_i^{NEOART} during the ELM cycle. (c) Thermo-currents of inner divertor used as ELM monitor.

The temperature profiles have been modelled using ASTRA in a predictive way. A prescribed χ profile is used as input and the heat transport equations are solved for T_i and T_e. The χ_i^{PB} profile determined via power balance analysis is used for the plasma core, while at the edge (ρ_{pol}>0.98) the neoclassical value is used. At the very edge of the plasma (ρ_{pol}>0.997), the neoclassical calculations provide unphysical results and therefore, χ_i^{PB} is implemented. The ELM is simulated by increasing χ_i to an anomalous value at the edge of the plasma. Here, the edge profile (ρ_{pol}>0.90) is multiplied by 10 for the time window [-0.3, 2] ms with respect to the ELM onset. The resulting modelled T_i profiles are shown in figure 5(a). Note that a time-dependent boundary condition for T_e and T_i at the separatrix is used. During the inter-ELM phase good agreement with the experimental values (marked by circles) is obtained, both before the ELM crash and during the recovery

phase after the ELM (t-t_{ELM}>3 ms). During the ELM crash itself, the ion heat transport is highly anomalous and requires non-linear MHD modelling.

3 Edge toroidal momentum transport analysis

Previous analysis of the H-mode edge rotation database at AUG showed a collisionality dependence of the edge impurity rotation [10]. Below a certain threshold in collisionality, the measured impurity toroidal rotation at the plasma edge changes sign from co- to counter-current (see also figure 1(c)). At the same collisionality value the neoclassical main ion poloidal rotation also changes sign from co- to counter-current. The behaviour of these two species, when used to calculate the main ion toroidal rotation via radial force balance and assuming a neoclassical main ion poloidal flow, leads to a nearly constant co-current main ion toroidal rotation. Hence, at low collisionality, due to a lack of frictional coupling, the main ion-impurity differential rotation can be quite large.
The behaviour of the toroidal rotation at low and high collisionality is modelled with ASTRA. Using torque balance analysis the torque density profiles are calculated with ASCOT [11] and TRANSP [13], which yield reasonable agreement at the plasma edge, consistent with previous studies [12]. ASCOT predicts an increased loss of beam particles at low collisionality leading to a negative j×B component due to an enhanced outward transport of beam ions (see figure 6). The toroidal field ripple (roughly 0.5% at the plasma edge of AUG) also gives an additional negative contribution for the net fast ion loss torque at the edge. The edge toroidal rotation is modelled with ASTRA using toroidal torque balance including diffusion, pinch and momentum sources (such as NBI and neutrals), while the neoclassical toroidal viscous torque and the torque due to turbulence driven residual stress were neglected. Due to the presence of poloidal impurity density asymmetries in the pedestal [14] the measured LFS toroidal rotation profile at the plasma edge is not representative for the flows on a flux surface [15, 16]. Thus, the flux surface averaged flows based on the LFS measurements and a fluid model [17] that was developed for describing the poloidal impurity density and rotation asymmetries [10], is used for the modelling. Comparison between the experimental profiles and the simulations shows good

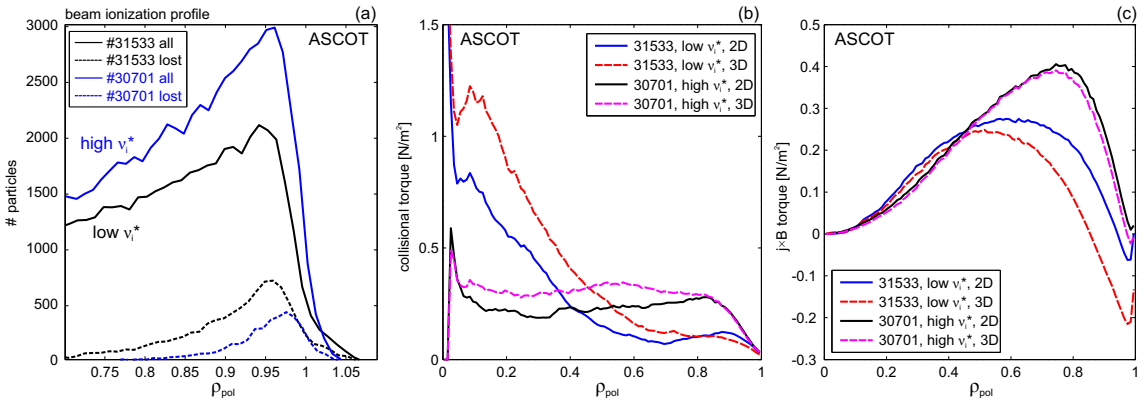

FIG. 6: (a) Beam ionization profile, (b) collisional and (c) $j \times B$ torque profiles.

agreement within the experimental uncertainties (see figure 7), indicating that diffusion and external momentum sources are the dominant players. The sign change of the impurity toroidal rotation observed at low collisionality can be explained by a negative edge torque combined with a large differential toroidal rotation, while the main ion toroidal rotation is almost unaffected.

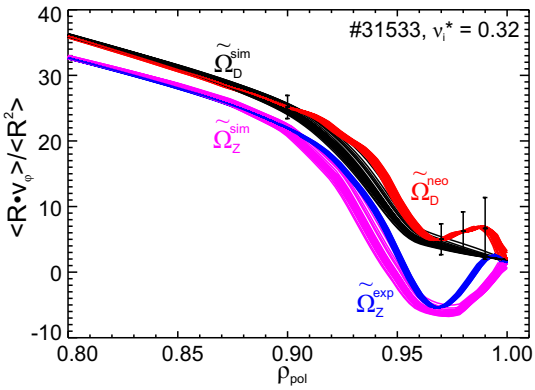

FIG. 7: Comparison of the experimental and simulated toroidal rotation of impurities (Z) and main ions (D). Note that the flux surface averaged flows $< R \cdot v_\phi > / < R^2 >$ *are plotted.*

4 Summary

Analysis of the inter-ELM ion heat transport in ASDEX Upgrade H-mode plasmas reveals that χ_i is close to the neoclassical level at both low and high collisionality. Charge exchange measurements with unprecedented time resolution (100 μs) at AUG revealed the dynamics of T_i during an ELM [8]. Using these measurements, the ion heat transport was analyzed during the entire ELM cycle. At the ELM onset, the ion heat transport is increased to anomalous values. The ion heat flux is first perturbed at the very plasma edge, the separatrix T_i increases leading to a reduced T_i gradient in the pedestal. Subsequently, the whole pedestal profile reduces during the ELM crash. The build-up of the T_i pedestal and the restoration of the ion heat transport to the pre-ELM neoclassical values is obtained 3–4 ms after the ELM.
The edge toroidal rotation is modelled using toroidal torque balance including diffusion, pinch and momentum sources (such as NBI and neutrals), while the neoclassical toroidal viscous torque and the torque due to turbulence driven residual stress were neglected. The fact that poloidal impurity density and flow asymmetries have been observed at the plasma edge of AUG has been taken into account in the model and the main ion toroidal rotation is evaluated by assuming that neoclassical theory describes the main ion poloidal flow. Comparison between the experimental flux surface averaged flows and the simulations shows good agreement within the experimental uncertainties. This suggests that diffusion and external momentum sources are the dominant player for the toroidal momentum at the plasma edge.

Acknowledgement This work has been carried out within the framework of the EUROfusion Consortium and has received funding from the European Union's Horizon 2020 research and innovation programme under grant agreement number 633053. The views and opinions expressed herein do not necessarily reflect those of the European Commission. The support from the EUROfusion Researcher Fellowship programme under grant number WP14-FRF-IPP/Viezzer and from the Spanish Ministry of Economy and Competitiveness (FJCI-201422139) is gratefully acknowledged.

References

[1] P. Gohil *et al.*, NF **38** 425 (1998)
[2] F. Ryter *et al.*, PRL **86** 5498 (2001)
[3] P. Mantica *et al.*, PRL **102** 175002 (2005)
[4] E. Wolfrum *et al.*, NF **55** 053017 (2015)
[5] G. V. Pereverzev *et al.*, IPP Report 5/98 (2002).
[6] E. Viezzer *et al.*, NF (in press).
[7] M. Cavedon *et al.*, NF (accepted).
[8] M. Cavedon *et al.*, in preparation.
[9] M. R. Wade *et al.*, PoP **12** 056120 (2005).
[10] E. Viezzer *et al.*, Nucl. Fusion **55** 123002 (2015).
[11] A. Snicker *et al.*, NF **53** 093028 (2013).
[12] O. Asunta *et al.*, CPC **188** 33-46 (2015).
[13] http://w3.pppl.gov/transp/
[14] E. Viezzer *et al.*, PPCF **55** 124037 (2013).
[15] T. Pütterich *et al.*, PRL **102** 025001 (2009).
[16] T. Pütterich *et al.*, Nucl. Fusion **52** 083013 (2012).
[17] E. Fable, private communication